

## Polymer brush under strong shear

Pik-Yin Lai\* and Chee-Yuen Lai

Department of Physics, National Central University, Chung-li, Taiwan 32054, Republic of China

(Received 25 March 1996; revised manuscript received 20 August 1996)

End-grafted polymer brush exposed to strong shear solvent flow is studied. Under strong enough shear flow, the shear force is nonlinear with the blob size depending on the shear force and not on the monomer volume fraction  $\phi$ . We derive the crossover force scale separating the weak and strong shear regime. The velocity profile of the flow,  $v(z)$ , inside and above the brush is calculated analytically by treating the flow as in a porous medium and solving the Brinkman equation. The solution of the velocity profile is then combined with nonequilibrium Monte Carlo simulation data, which allow a self-consistent determination of the chain end-to-end length and the incline angle of the chain. We derive the scaling form for the chain positions  $x(n)$  for the  $n$ th monomer and verified by our simulation data. We further obtain analytical expression for  $x(n)$  in terms of the effective viscosity of the model. [S1063-651X(96)07812-9]

PACS number(s): 36.20.-r, 47.50.+d, 83.20.Jp

### I. INTRODUCTION

In recent years, the structure and dynamics of end-grafted polymers under the action of flow fields have drawn a lot of research interest both experimentally [1–3] and theoretically [4–10]. One major reason for the growing research interest on such end-grafted polymer layers is that the interaction between these grafted surfaces can be modified in a more or less controlled way. In particular, the behavior of two surfaces grafted with polymers in shear motion [11–13] has received much interest because of its important applications in friction control and adhesion. A crucial aspect of these applications is the structure of these polymer layers under the flow of the fluid in the processes involved. A knowledge of this structure would also provide some understanding of the fundamental mechanism of interfacial friction and adhesion on a molecular level. The understanding of such layers exposed to shear flow is very limited; previous studies have focused on the structure of a polymer brush under relatively weak shear [4–8,10]. When the shear rates are not strong, the scaling rules for the blob picture in the semidilute regime still hold, i.e., the blob size  $\xi(\phi)$  is determined [14] by the monomer volume fraction  $\phi$ . However, under strong enough shear, the blob size depends on the shear force and not on  $\phi$  (see Fig. 1) and thus would produce nonlinear responses [15] that may affect the brush strongly.

### II. MODEL AND SIMULATION METHOD

The bond-fluctuation model (BFM) [16] for polymer chains is used in the simulation. Monodispersed end-grafted polymers (each consisting of  $N$  monomers) are placed inside an  $L \times L \times M$  box where one  $L \times L$  plane ( $xy$  plane) is an impenetrable grafting wall. Periodic boundary conditions are chosen in the  $x$  and  $y$  directions and  $M$  is chosen to be large enough so that it will never affect the configurations of the grafted chains. The chain lengths cover a range of

$10 \leq N \leq 60$ . Several suitable grafting densities are chosen at which the systems are well in the brush regime. The effect of shear flow in the  $+x$  direction is implemented by a viscous force acting on a monomer,

$$F^x = \eta a v(z), \tag{1}$$

where  $\eta$  is a constant which can be interpreted as an effective viscosity and  $a$  is the monomer size. This net viscous force physically arises from the impact on the monomer by the random (but with a net flow in the  $+x$  direction) motions of the solvent molecules. Due to this force, the excess probability of a monomer moving in the  $+x$  direction is enhanced by an amount proportional to the force with

$$p_x - p_{-x} = C(F^x a / (kT)) \tag{2}$$

for some dimensionless constant  $C$ , where  $T$  is the temperature and  $k$  is the usual Boltzmann constant. Hence the shear flow can be modeled once the velocity profile  $v(z)$  is known. The probabilities of a monomer moving in other directions  $\pm y, \pm z$  are taken to be unchanged. It follows from Eqs. (1)

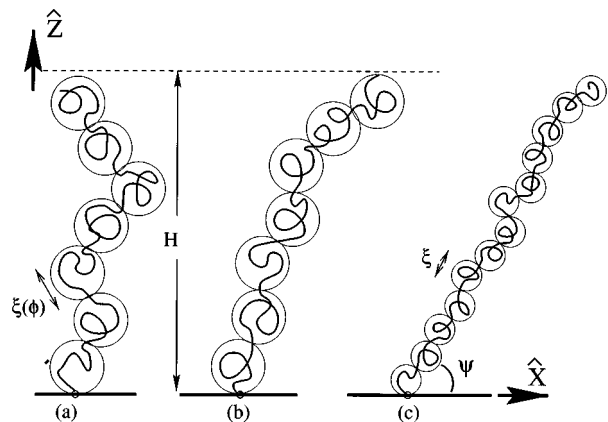


FIG. 1. Schematic illustrations of the blob pictures for the configurations of end-grafted polymer brush in (a) no shear, (b) weak shear, and (c) strong shear regimes.  $\psi$  is the angle between the center of mass direction and the  $x$  axis.

\*Author to whom all correspondences should be addressed. Electronic address: pylai@phyast.phy.ncu.edu.tw

and (2) that  $p_{+x} - p_{-x} \propto v(z)$  and in practice this proportional constant is chosen such that even for the longest chain in our studies in its fully extended configuration,  $p_{+x} < 1/3$  still holds. For the case of a semidilute polymer brush, the reaction of polymers would change the flow profile and one expects that some sort of screening occurs that diminishes the velocity of flow inside the brush. Following previous studies [6,8] the grafted layer is treated as a porous medium with pore size given by the hydrodynamic screening length  $\approx \xi$  in a semidilute polymer solution [17]. The velocity profile of solvent flow can be obtained by solving the Brinkman equation [18] at constant pressure,

$$\frac{d^2 v}{dz^2} = \frac{v}{\xi^2}. \quad (3)$$

For the case of weak shear [8] [Fig. 1(b)], the blob size is determined by the local monomer concentration [14] via  $\phi(z) = [a/\xi(z)]^{3-1/\nu}$ , where  $\nu$  is the usual self-avoiding walk exponent which was taken to be  $\nu = 3/5$  for analytical calculations and  $\nu \approx 0.588$  when it is used in interpreting simulation data.  $v(z)$  and  $\phi(z)$  can then be determined self-consistently from Eq. (3) and the simulation data as described in detail in Ref. [8]. However, the shear force increases up to the point that the blob size  $\xi$  no longer depends on  $\phi$  but instead is determined by the shear force in the strong shear Pincus regime. According to Pincus's theory, the blob size in the Pincus regime is determined by the applied force  $F$  as [15]  $F\xi \approx kT$ . And if the chain is composed of  $N_b$  blobs, then one has  $\xi \approx a(N/N_b)^\nu$ . For a large enough applied force [as in Fig. 1(c)] in the Pincus regime (with  $aN^\nu < R_e \ll aN$ ), the end-to-end distance  $R_e$  is given by  $R_e \approx \xi N_b$ . Hence

$$\xi = a(Na/R_e)^{\nu/(1-\nu)} = a(Na/R_e)^{3/2} \quad (4)$$

and  $R_e = Na(Fa/kT)^{(1-\nu)/\nu}$ . Thus in the strong shear case of the Pincus regime,  $\xi$  is independent of  $z$ . Suppose the height of the polymer brush is  $H$  and denote the regions inside ( $0 \leq z \leq H$ ) and above ( $z \geq H$ ) the brush by subscripts *I* and *II*. Equation (3) is solved analytically with the boundary conditions  $v_I(0) = 0$ ,  $v_{II}(z \rightarrow \infty) = \gamma z$ ,  $v_I(H) = v_{II}(H)$ , and  $(dv_I/dz)|_H = (dv_{II}/dz)|_H$ . The solution is

$$v_I(z) = \frac{\gamma \xi \sinh(z/\xi)}{\cosh(H/\xi)} \quad (5)$$

and  $v_{II}(z) = \gamma[z - H + \xi \tanh(H/\xi)]$ . An important consequence of the solution is that the flow profile above the brush is quite strongly affected by the presence of a polymer layer below. The present solution of  $v(z)$  is superior when compared with previous studies in that it has no kink in  $v(z)$  at  $z = H$  ( $v$  has a kink in Ref. [8]) and gives the correct boundary condition at  $z = \infty$ :  $v(z \rightarrow \infty) = \gamma z$ . On the other hand, the brush height is related to the chain length via  $H = R_e \sin\psi$ , where  $\psi$  is the tilted angle as shown in Fig. 1(c).  $R_e$  and  $\sin\psi$  are regarded as parameters to be determined self-consistently from the Monte Carlo data as follows: starting from an arbitrary set of values of  $(R_e, \sin\psi)$ ,  $v(z)$  is calculated from Eqs. (4) and (5). The  $v(z)$  so calculated is then used in the simulation and an improved estimate of

$(R_e, \sin\psi)$  is then measured. The improved  $(R_e, \sin\psi)$  is in turn used as the new input in the next simulation and this procedure is repeated until the input  $(R_e, \sin\psi)$  is consistent with the output estimate. In practice, we find that only very few iterations are needed to obtain the self-consistent  $(R_e, \sin\psi)$ .

The crossover force scale  $F^*$  separating the weak and strong shear regimes can be easily derived from  $F^* \xi(\phi) = kT$  and using  $\phi = (a/\xi)^{3-1/\nu}$ . One gets  $F^* a/(kT) = \phi^{\nu/(3\nu-1)} = \phi^{3/4}$ . The present simulations concentrate on the strong shear regime as specified by the Pincus regime.

### III. RESULTS

We find that [19] the response of the grafted chain to the shear flow is to incline in the direction of flow, but at the same time unfolding the chain segments such that the end-to-end distance increases and the brush height is essentially unaltered. This result is in agreement with the case of weak shear studied in Ref. [8].

In the case of no shear the average  $z$  position of the  $n$ th monomer along a chain is given by [20,21]

$$z(n) = z(N) \sin[n\pi/(2N)] \quad (6)$$

from self-consistent field theory and the brush height is

$$H \equiv z(N) = bN\sigma^{(1/\nu-1)/2} = bN\sigma^{1/3} \quad (7)$$

with the proportional constant  $b \approx 1.76$  for the BFM [22]. Our data [19] indicate that Eqs. (6) and (7) still hold approximately in the strong shear Pincus regime unless the shear rate is extremely large.

At equilibrium, the elastic deformation force must be equal to the viscous force due to the shear flow. Assuming the elastic free energy can still be taken to be Gaussian and denoting the  $x$  position of the  $n$ th monomer by  $x(n)$ , we thus have

$$\frac{kT}{a^2} \frac{d^2 x(n)}{dn^2} = -F^x = -\eta a v_I[z(n)], \quad (8)$$

where  $\eta$  is a constant which can be interpreted as an effective viscosity. Using Eqs. (4) and (5), one can easily deduce that  $x(n)$  has the functional form

$$x(n) = -\gamma N^3 \sigma^{1/3} B[u, n/N], \quad (9)$$

where  $u \equiv N\sigma^{5/6}/\sin^{3/2}\psi$  and  $B$  is some scaling function. This is tested in a scaling plot in Fig. 2 with  $n = N/2$  for various values of  $\sigma$ ,  $\gamma$ , and  $N$ . The data show a rough collapse suggesting the validity of the proposed scaling form. In fact, Eq. (8) can be solved directly with the boundary conditions  $x(0) = 0$ ,  $(dx/dn)|_N = 0$ :

$$x(n) = -\frac{\eta \gamma N \sigma^{1/3} a^3 b}{kT w \cosh w} \int_0^n \int_N^{n'} \sinh \left[ w \sin \left( \frac{n\pi}{2N} \right) \right] dn'' dn', \quad (10)$$

where  $w \equiv (b/a)^{5/2} u$ . The above integral can be evaluated numerically if  $\sin\psi$  is known, which can be measured from our simulation data  $\langle \sin\psi \rangle$ . Thus for given values of  $\sigma$  and

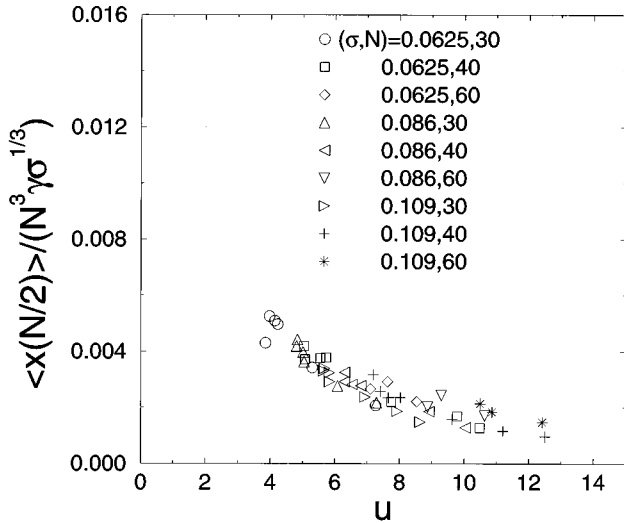


FIG. 2. Scaling plot of  $\langle x(N/2) \rangle / (N \gamma \sigma^{1/3})$  versus  $u$  for various values of  $\sigma$  and  $N$ .  $u \equiv N \sigma^{5/6} \langle \sin \psi \rangle^{-3/2}$ .

$N$ , if we take  $\sin \psi \approx \langle \sin \psi \rangle$ , the right-hand side of Eq. (10) can be evaluated except the constant  $\eta/kT$ . On the other hand, the left-hand side of (10) can be obtained from simulation data:  $x(n) \approx \langle x(n) \rangle$ . Hence the constant  $\eta$  can be estimated. For various values of  $\sigma$ ,  $\gamma$ , and  $n$ ,  $\eta a^2/kT \approx 0.02 \pm 0.005$  is roughly a constant. The physical meaning of  $\eta$  is an effective viscosity in the BFM. As a by-product, the proportional constant in Eq. (2) governing the nonequilibrium Monte Carlo (NEMC) method in the BFM can also be estimated once  $\eta a^2/(kT)$  is known. We find  $C \approx 0.14$ .

$x(n)$  computed from (10) using this value of  $\eta$  agrees rather well with the corresponding data of  $\langle x(n) \rangle$  as illustrated in Fig. 3 for two different shear rates. Furthermore, one can estimate the  $x$  position of the end monomer from simple geometry and get

$$x(N) = H(1 - \sin^2 \psi)^{1/2} / \sin \psi. \quad (11)$$

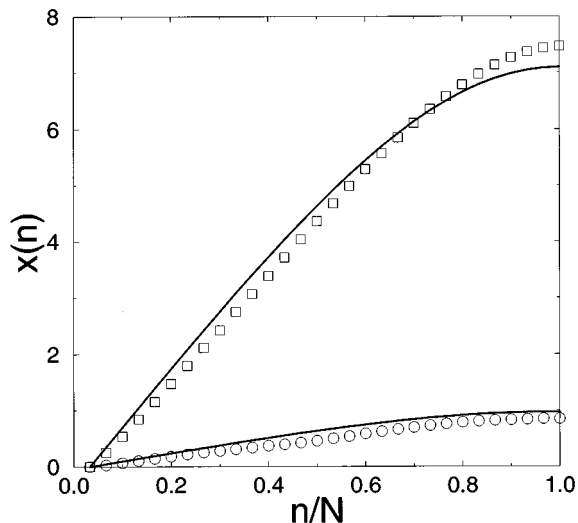


FIG. 3.  $x(n)$  versus  $n/N$  at  $\gamma=0.01$  ( $\circ$ ) and  $0.08$  ( $\square$ ) for  $\sigma=0.0625$  and  $N=30$ . Symbols are simulation data and the solid curves are analytic results obtained from (10).

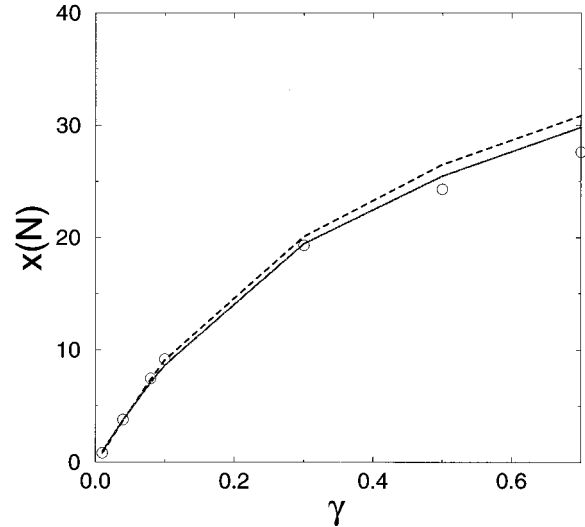


FIG. 4. End position,  $x(N)$ , as a function of  $\gamma$  for  $\sigma=0.0625$ ,  $N=30$ . Symbols are simulation data, solid and dashed curves are computed from (10) and (11), respectively.

With Eq. (11),  $x(N)$  can be computed if we again take  $\sin \psi \approx \langle \sin \psi \rangle$ . Values for the end-monomer position evaluated from (10) and (11) together with those measured directly from simulations are all displayed in Fig. 4 for comparison. We find that all of them agree reasonably well except at extremely strong shear rates.

#### IV. DISCUSSION AND OUTLOOK

Our present simulation results are consistent with all known previous simulation results [8–10] using different methods so that the brush height stays almost constant upon shear. No swelling of the brush thickness under shear solvent flow was observed in our simulations. These results should be compared with the force experiments by Klein *et al.* [11], which measured the normal force between two polymer brushes immersed in a solvent that were sheared against each other by a periodic drive. When the relative speed of sliding exceeds some critical value, a strong normal repulsive force sets in between the brushes, even when the separation of the brushes exceeds the range of repulsion in the absence of shear. This result has been interpreted as an increase in brush thickness when the solvent flows through it. On the theoretical side, analytical calculation by Rabin and Alexander indicated that the brush height remained unaltered [4] for a single brush under shear. Subsequently, Barrat [5] revisited their calculations and claimed that there is an increase in brush thickness upon shear. However, it has been recently pointed out [10] that the “brush swelling” prediction in Barrat’s calculation is an artifact due to an underestimate of the brush thickness in the limit of zero shear. Finally, Kumaran [7] analyzed the hydrodynamic interactions of a single brush under solvent flow and suggested that the tilting of the brush could cause an asymmetric pair distribution of the monomers. As a result, a flow of solvent in a direction normal to the shear can be created and hence an increase in the brush thickness occurs.

On the other hand, nearly all the computer simulations on polymer brushes under shear [8,10], including the present

one and the above mentioned analytical studies, contained no real hydrodynamics (in the sense of having explicit solvent molecules and backflow, etc.), although *hydrodynamic interactions* were approximated by an asymmetric jump rate of the monomer with the use of the Navier-Stokes-type equation to calculate the flow profile self-consistently. And none of these simulations indicate a swelling of brush thickness upon shear. Hydrodynamic interactions such as those described by the Oseen tensor, which couples flows between different directions, could produce the swelling of the layer in the  $z$  direction. Moreover, even a very recent nonequilibrium molecular dynamic simulation on two brushes (of rather short chain lengths) shearing against each other with explicit solvent molecules [9] *did not* indicate an increase in the layer thickness. Periodic boundary conditions were used in this simulation and the shear was unidirectional in contrast to the conditions in the force experiment [11] of a hard wall boundary of the container and the oscillating drive for shear motion.

At this point, there is still no clear reason for the discrepancies between the simulation results and the experiments. One possible cause for the disagreement may be due to the surface corrugation that would produce a flow component perpendicular to the solvent flow direction [2,8]. Another possibility may originate from the complicated flow pattern that might result from the oscillating drive for shear motion in the force experiment. Since the two brushes are immersed in a finite container and the periodic shear drive could cause strong hydrodynamic backflow, depending on the frequency

of the drive and the intrinsic relaxation time scales of the polymer and solvent, a flow component of the solvent perpendicular to the shear motion might be induced. The latter possibility can be clarified by direct experimental measurements on the brush thickness of a single brush under shear solvent flow using neutron scattering. We believe that the apparent increase in the repulsion range between the two brushes sheared against each other has a hydrodynamic and dynamic origin. To achieve a deeper understanding of the force experiment results, molecular dynamic simulations of two brushes shearing against each other driven periodically with a sufficient number of explicit solvent molecules placed in a hard wall container should provide very valuable information on the mechanism of the apparent brush thickening phenomenon, but the computing power for such a study would be very demanding. Nevertheless, our NEMC method provides a rather convenient route in the study of polymer chain under hydrodynamic flow and it also determines the effective viscosity and proportional constant  $C$  for NEMC in the BFM. These model dependent parameters are very useful and give a directly physical interpretation of the NEMC method, which is applicable to other systems of polymer under flow, such as polymer migration and flow induced rheology studies.

#### ACKNOWLEDGMENTS

We thank the National Council of Science of Taiwan for support under Grant No. NSC 85-2112-M-008-016.

- 
- [1] Y. Cohen, *Macromolecules* **21**, 494 (1988).  
 [2] M. Bagassi, G. Chauveteau, J. Lecoutier, J. Englert, and M. Tirrell, *Macromolecules* **22**, 262 (1989).  
 [3] R. S. Parnas and Y. Cohen, *Macromolecules* **24**, 4646 (1991).  
 [4] Y. Rabin and S. Alexander, *Europhys. Lett.* **13**, 49 (1990).  
 [5] J.-L. Barrat, *Macromolecules* **24**, 832 (1991).  
 [6] S. Milner, *Macromolecules* **24**, 3704 (1991).  
 [7] V. Kumaran, *Macromolecules* **26**, 2464 (1993).  
 [8] P.-Y. Lai and K. Binder, *J. Chem. Phys.* **98**, 2366 (1993).  
 [9] G. H. Peters and D. J. Tildesley, *Phys. Rev. E* **52**, 1822 (1995).  
 [10] L. Miao, H. Guo and M. J. Zuckermann, *Macromolecules* **29**, 2289 (1996).  
 [11] J. Klein, D. Perahia, and S. Warburg, *Nature (London)* **352**, 143 (1991).  
 [12] J. Klein, Y. Kamiyama, H. Yoshizawa, J. N. Israelachvili, G. H. Fredrickson, P. Pincus, and L. J. Fetters, *Macromolecules* **26**, 5552 (1993).  
 [13] H. Yoshizawa, Y.-L. Chen, and J. N. Israelachvili, *J. Phys. Chem.* **97**, 4129 (1993); **97**, 11 300 (1993).  
 [14] P. G. de Gennes, *Scaling Concepts of Polymer Physics* (Cornell University Press, Ithaca, 1979).  
 [15] P. Pincus, *Macromolecules* **9**, 386 (1976).  
 [16] I. Carmesin and K. Kremer, *Macromolecules* **21**, 2819 (1988); *J. Phys. (Paris)* **51**, 915 (1990); H-P. Deutsch and K. Binder, *J. Chem. Phys.* **94**, 2294 (1991).  
 [17] D. Richter, K. Binder, B. Ewen, and B. Stühn, *J. Phys. Chem.* **88**, 6618 (1984).  
 [18] H. C. Brinkman, *Appl. Sci. Res.* **A1**, 27 (1947).  
 [19] More simulation results will be published elsewhere.  
 [20] S. T. Milner, T. A. Witten, and M. E. Cates, *Europhys. Lett.* **5**, 413 (1988); *Macromolecules* **21**, 2610 (1988).  
 [21] A. M. Skvortsov, A. A. Gorbunov, I. V. Pavlushkov, E. B. Zhulina, O. V. Borisov, and V. A. Priamitsyn, *Polymer Science USSR* **30**, 1706 (1988).  
 [22] P.-Y. Lai and E. B. Zhulina, *J. Phys. (France) II* **2**, 547 (1992).